ChemComm



COMMUNICATION

View Article Online

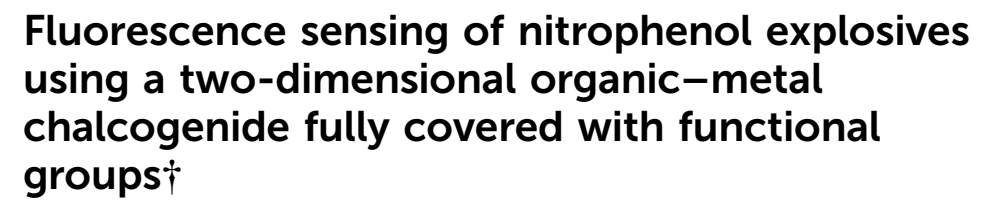


Cite this: Chem. Commun., 2022, **58**, 4615

Received 10th February 2022, Accepted 9th March 2022

DOI: 10.1039/d2cc00834c

rsc.li/chemcomm





A new 2D fluorescent organic-metal chalcogenide (OMC), CdClHT (HT = 4-hydroxythiophenol), evenly covered with phenol groups is reported. CdClHT represents unparalleled selectivity and the highest sensitivity towards 2,4,6-trinitrophenol (TNP) (K_{SV} = 2.16 \times 10^7 m^{-1} , experimental LOD = 2 nM), among all reported 2D conjugated polymer (CP) luminescent detectors.

Since the discovery of graphene in 2004, two-dimensional (2D) nanomaterials have attracted considerable interest owing to their novel chemical and physical properties, such as their 2D layered structure, good conductivity, high mechanical stability, and facile functionalization. 1-3 2D luminescent materials can respond to external stimuli quickly and easily because of their higher specific surface area properties, which can provide more active sites for binding analytes. Besides, surface chemistry in 2D materials such as functional surfaces, chemical modification and surface catalytic reactions are effective strategies to improve the performance of 2D materials.4,5 Luminescence could also be tuned by selected chemical functionalization. Their diversity in chemistry and structure offer an immense opportunity to selectively analyze analytes ranging from gases to metals and biological molecules.^{3,6}

Recently, great efforts have been devoted to developing new fluorescent materials with various sensing mechanisms for detecting explosives in order to achieve great sensitivity and selectivity, as well as fast response time. ⁷⁻¹⁰ As we all know, covalently bonding or physically adsorbing organic molecules to 2D materials can introduce functions related to organic molecules into 2D materials, which affords favorable affinity for target chemicals. 11-13 Therefore, organic modification is a promising way to increase the fluorescence efficiency and

A new type of functional 2D material, organic-metal chalcogenides (OMCs), has been constructed through coordination assembly. 14,15 Unlike the E-M strategy, the surfaces of OMCs are fully and orderly covered by organic functional groups, which can effectually enhance their interaction with analytes. For example, an OMC, CuHBT (HBT = 4-hydroxythiophenol), was revealed that compared with other 2D materials and their composite materials showed magnificent intrinsic peroxidaselike catalytic activity and reflected the lowest detection limit in the detection of glucose by fully covered phenol groups acting as "promoters". 14 Besides, Ag(SPh-NH2), with fully and orderly covered -NH2 groups as "receptors", exhibited the highest sensitivity, excellent selectivity and reversibility in response to NO₂ among all the reported 2D chemiresistive sensing materials at room temperature (RT).16 These examples convincingly prove that OMCs can possess higher sensitivity as one type of chemical sensing material at RT. Recently, a few OMCs with d¹⁰ coinage metals have regained interest due to their appealing photoluminescence properties. 17-20 Despite the fact that there are some examples of temperature sensors based on luminescent OMCs, 21-23 none has been utilized to detect molecules using potential functional groups adequately on luminescent OMCs.

Trinitrophenol (TNP) as an intermediate of dyes is widely used in industry, pesticides, explosives and so on.²⁴ The detection of TNP is important due to its danger, toxicity and difficulty to degrade in nature.25,26 Since the TNP molecule not only has electron-deficient nitro groups but also hydroxyl groups, ascertaining the value of hydroxyl groups in the TNP structure is very important for TNP-related explosives detection.^{27,28} Hence, following our research interest in luminescent OMCs fully covered with hydroxyl groups based on

selectivity of the analytes. However, reported methods mainly focus on the modification of organic molecules on preexfoliated nanosheets (exfoliation and then organic modification (E-M) strategy). As a result, the surface functionalization process is normally destructive and the organic groups on 2D materials are usually not homogeneously distributed, which hinders the application of these materials.

^a State Key Laboratory of Structural Chemistry, Fujian Institute of Research on the Structure of Matter, Chinese Academy of Sciences (CAS), No. 155 Yangqiao Road West, Fuzhou, Fujian, 350002, P. R. China. E-mail: gxu@fjirsm.ac.cn

^b University of Chinese Academy of Sciences (UCAS), No. 19A Yuquan Road, Beijing 100049, P. R. China

[†] Electronic supplementary information (ESI) available: Experimental details, Fig. S1-S13 and Tables S1-S2. See DOI: 10.1039/d2cc00834c

Communication ChemComm

organosulfur ligands, herein, a new fluorescent OMC, CdClHT, was prepared through coordination assembly to detect TNP. The 2D $\{CdClS\}_n$ layers of CdClHT are covered by ordered phenol groups on both sides. This unique 2D material architecture significantly enhances the interaction between the CdClHT nanosheets and analytes and thus promotes electron transfer in chemical applications. As expected, photoluminescence (PL) studies showed that the same green-light emission was observed in bulk crystals, few-layer nanosheets and the nanosheets in the solvent. In particular, CdClHT nanosheets in ethanol solution represent high fluorescence quenching efficiency toward nitrophenol (TNP, DNP, NP), which can distinguish analytes with similar structures (such as TNT, TNP). The limit of detection (LOD) of TNP was found to be 2 nM, which is almost the lowest LOD in 2D CPs, including COFs and MOFs. 29,30 Furthermore, CdClHT shows the highest K_{SV} value toward TNP among the reported 2D luminescent CPs.

A 2D OMC Cd₃Cl₂(HT)₄ (1) with functional group surface covering was synthesized using 2(CdCl₂)·5(H₂O) and HT ligand (Fig. 1a). The detailed description is shown in the Supporting information. X-ray diffraction showed that compound 1 belongs to the $P2_1/c$ space group. As shown in Fig. 1b, each Cd atom forms a 6-coordination structure with two μ₃-bridging Cl atoms and four μ_3 -bridging S atoms. Each {CdClS} octahedron connects with others through edge-sharing to form a 2D $\{CdClS\}_n$ layer. The bond length of Cd-S is between 2.630-2.749 Å, and the bond length of Cd-Cl is between 2.656-2.842 Å. More interestingly, in this layer, cis-octahedra are adjacent to trans-octahedra where Cl is placed in different positions (Fig. S1, ESI \dagger). The {CdClS}_n layer is further connected with phenol groups through C-S covalent bonds to form a sandwich structure as a supermolecule multi-quantum well structure. Simultaneously, for the doping of Cl atoms and the steric hindrance of the connection type in the layer, benzene from the ligand of 1 shows a parallel and vertical stacking model as shown in Fig. 1b, rather than the completely regular arrangement in our previous works. 14,16,31 These mono-layers

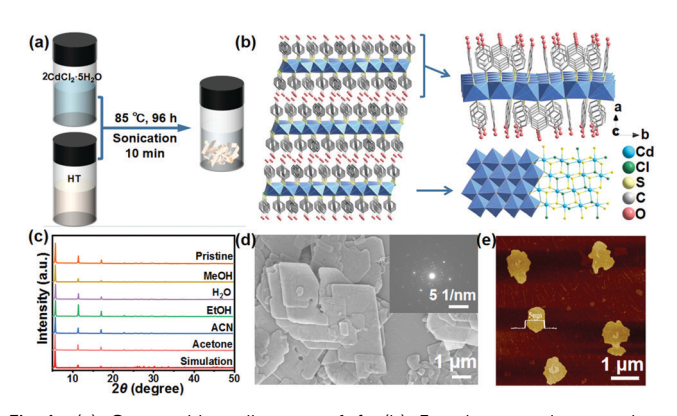


Fig. 1 (a) Composition diagram of 1. (b) Few-layer and mono-layer structures of 1. Hydrogen atoms have been omitted for clarity. (c) Experimental and simulated PXRD patterns of 1 and PXRD patterns after immersion in different solvents for 24 h. (d) SEM image of few-layer 1; the inset is its selected area electron diffraction pattern. (e) Typical AFM image of few-

parallel pack with each other along the a axis forming few-layer Cd₃Cl₂(HT)₄, which produces a clear superlattice alignment with periodically stacked inorganic and organic sublattices (Fig. 1 and Fig. S2, ESI†).

The experimental powder X-ray diffraction (PXRD) pattern of 1 is in good agreement with its simulated one, verifying its phase purity (Fig. 1c). Compared with HT ligand, Fourier transform infrared spectroscopy (FT-IR) (Fig. S3, ESI†) shows the disappearance of the mercaptan bond frequency at \sim 2550 cm⁻¹, which testifies to the successful coordination of HT ligands with metal salts. Meanwhile, the stretching frequency observed in 1 ($\sim 3300 \text{ cm}^{-1}$) proves the existence of hydroxyls without coordination, which provided sufficient potential active sites for the detection of TNP. The red shift of the hydroxyl peak also further confirms the hydrogen bond between the layers of the structure 1. Scanning electron microscopy (SEM) measurements reveal the nanobelt morphology of the as-prepared few-layer 1 with a length and width of several micrometers (Fig. 1d). The selected area electron diffraction pattern of TEM shows sharp and ordered spot arrays, indicating the good crystallization of few-layer 1 (inset of Fig. 1d). In order to fully expose functional groups to improve detection performance, we obtained nanosheets with a thickness of ~ 5 nm by ultrasonic mechanical stripping (Fig. 1e). Moreover, to support further application, we examined the chemical stability of compound 1 nanosheets. The samples were checked in common solvents. As shown in Fig. 1c, the nanosheets remain intact after immersion in different solvents for 24 h. Meanwhile, the samples are thermally stable up to 312 °C in N2 (Fig. S4, ESI†). These results indicate that the compound 1 is feasible for practical applications.

The PL spectrum of the powder sample exhibits emission centered at 550 nm when excited at 340 nm (Fig. S5, ESI†). It can be seen from the CIE coordinate diagram that the emission color is green (Fig. S6, ESI†). Considering that surface functional groups can provide better dispersion in solvents, 11 nanosheets were dispersed in various solutions under ultrasonic conditions. As shown in Fig. S7, the stripped nanosheets can be evenly dispersed in ethanol, without precipitating after standing for 48 h. Most anticipated is that the fluorescence emission of the dispersion is consistent with that of the powder (Fig. S8, ESI†). Therefore, we tried to explore its role in the detection of nitro explosives by fluorescence sensing, given its excellent stability, dispersibility in ethanol and fully covered surface by functional groups.

Considering that TNP is one of the most dangerous chemicals and its explosive nature is even stronger than TNT among all nitroaromatic explosives, the highly sensitive and selective detection of TNP is urgently demanded. As a demonstration, compound 1 exhibited efficient sensing performance toward TNP. The fluorescence intensity of compound 1 was promptly quenched from 2.6% to 90.7%, as the amount of TNP dropped from 2 nM to 280 nM (Fig. 2a and Fig. S9, ESI†). The quenching efficiency was further analyzed by the Stern-Volmer equation, $(I_0/I) = K_{SV}[A] + 1$, where I_0 is the initial fluorescence intensity before the addition of analyte, I is the fluorescence intensity in

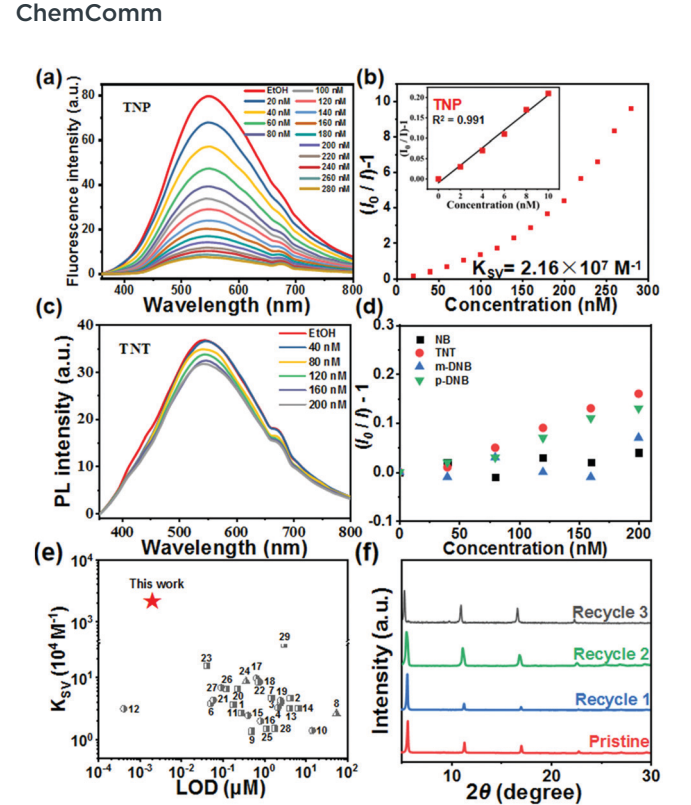


Fig. 2 (a) Effect on the emission spectra of 1 dispersed in EtOH upon incremental addition of TNP. (b) SV plots of TNP. (c) Effect on the emission spectra of 1 dispersed in EtOH upon incremental addition of TNT. (d) SV plots of other nitroaromatic explosives (NB, TNT, m-DNB, p-DNB. (e) A comparison of K_{SV} and LOD with reported 2D luminescence CPs (for details, see Table S1, ESI†). (f) PXRD patterns of 1 after detecting 200 nM TNP

the presence of analyte, [A] is the molar concentration of analyte, and K_{SV} is the quenching constant (M⁻¹). As shown in Fig. 2b, the fluorescence quenching shows a good linear relationship when the concentration of TNP is lower than 10 nM while the SV curve shows an upward curve with the increase of the concentration of the analyte, indicating the possibility of self-absorption or an energy-transfer process.³² Compound 1 has the highest calculated K_{SV} value of 2.16 \times 10⁷ M⁻¹ toward TNP among the reported 2D luminescence CPs (Fig. 2e and Table S1, ESI†). What's more, the experimental detection limit of 1 toward TNP is 2 nM, which is far lower than the theoretical LOD of TNP among almost all reported 2D CPs, including COFs and MOFs (Fig. 2e and Table S1, ESI†). As a comparison, the fluorescence of compound 1 was only quenched by 13% when 200 nM TNT was dropped, as well as other nitroaromatic explosives, m-DNB, NB and p-DNB (Fig. 2c and 2d). This proved unparalleled selectivity of compound 1 toward TNP among nitroaromatic explosives. PXRD confirmed that after fluorescence titrations with 3 recycles, the compound still maintains structural integrity (Fig. 2f).

Motivated by the above results: though there is only one position difference between TNT and TNP in their structures, a hydroxyl substituent for TNP while a methyl substituent for TNT, the former displays an almost 6 times higher quenching

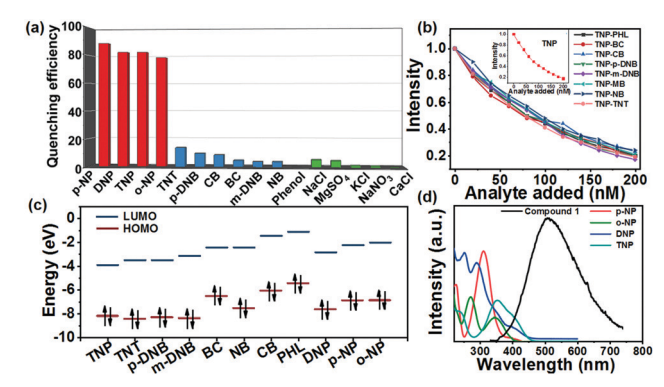


Fig. 3 (a) Percentage of fluorescence guenching obtained for different 200 nM analytes at RT. (b) Decrease in percentage of fluorescence intensity upon the addition of 1 in EtOH of different nitro compounds followed by TNP. (c) HOMO and LUMO energies for explosive analytes and other benzene interferents. (d) Spectral overlap between the absorption spectra of the analytes and the emission spectrum of 1 in EtOH.

efficiency compared to TNT, indicating that the hydroxyl group of TNP has a great contribution for the good selectivity. To further confirm such results, other hydroxyl-containing nitroaromatics and aromatics with single functional groups, such as p-nitrophenol (p-NP), o-nitrophenol (o-NP), DNP, CB, BC and phenol were titrated for performing fluorescence quenching. Interestingly, compound 1 showed significant quenching efficiencies toward p-NP (95.2%), o-NP (86.8%) and DNP (90.5%) and the calculated K_{SV} values of DNP, p-NP and o-NP were $2.31 \times 10^7 \text{ m}^{-1}$, $1.64 \times 10^7 \text{ m}^{-1}$ and $1.51 \times 10^7 \text{ m}^{-1}$, respectively, which are comparable to TNP (Fig. S10, ESI†). However, just slight quenching was observed with addition of analytes with single functional groups of nitro such as DNP, CB, BC and phenol (Fig. 3a and Fig. S11, ESI†). This result further demonstrates that only the synergistic effect between the hydroxyl and nitryl groups of the analytes promotes efficient fluorescence detection. In addition, the selectivity of 1 toward common metal ions (Fig. 3a and Fig. S12, ESI†) and TNP in the presence of other aromatic compounds has been studied. As shown in Fig. 3b, the stepwise decrease in fluorescence intensity clearly demonstrates the unprecedented selectivity of 1 toward TNP even in the presence of other aromatic compounds with a high concentration (200 nM).

In order to better understand the fluorescence quenching effect of 1 toward nitroaromatics with different functional groups, the quenching mechanism was proposed. Generally, the proposed mechanism of fluorescence quenching effect includes photo-induced electron transfer, 33,34 resonance energy transfer,³⁵ and intermolecular charge transfer pathways.^{36,37} The HOMO and LUMO orbital energies of aromatic compounds were calculated by density functional theory at the B3LYP/ 6-31G* level (Fig. 3c and Table S2, ESI†). Obviously, the order of LUMO energy profile of nitroaromatics was generally in good accordance with the order of quenching efficiency toward these analytes. However, the order of observed quenching efficiency is not fully in concurrence with the LUMO energies of DNP, p-NP and o-NP. This designates that the photo-induced electron

transfer is not the only mechanism for fluorescence quenching of 1 toward nitrophenol.

Communication

As mentioned above, the non-linear S-V plot for TNP suggests an energy transfer mechanism. Resonance energy transfer can dramatically enhance the fluorescence-quenching efficiency and also improves sensitivity. 38,39 As shown in Fig. 3d, the emission peak of 1 has a spectral overlap with the absorption spectrum of nitrophenols, so the efficient quenching occurs by an energy transfer mechanism, which leads to a higher quenching response. Compared with electron transfer of short-range processes, energy transfer as a long-range process could effectively quench the emission by carrying over the surrounding fluorophores to amplify the quenching response of 1. That is why 1 responds more sensitively toward TNP than other nitroaromatic explosives whose absorption spectrum has no spectral overlap with the emission band of 1 (Fig. S13, ESI†). Meanwhile, the existence of hydrogen-bonding interactions might enhance the absorption and the intermolecular charge transfer between 1 and hydroxyl-containing nitroaromatics. These results give powerful proof that the selective detection of TNP explosive was through synergistic effects including electron transfer, energy transfer and hydrogen-bonding interaction.

In conclusion, a 2D fluorescent OMC, organic-inorganic hybrid superlattice CdClHT has been reported. Thanks to surface-decorated organic functional groups, CdClHT nanosheets presented magnificent sensitivity, the highest Ksv value and almost the lowest LOD towards nitroaromatic explosive TNP at RT among all reported 2D materials. Remarkably, the compound exhibited extraordinary selectivity toward TNP among nitroaromatic explosives. The selectivity was mainly ascribed to multiple synergism of electron and energy transfer between TNP and 1. This work not only provides a new insight into the design of fluorescent organic-metal chalcogenides but also demonstrates the feasibility of enhancing the sensitivity and selectivity of explosives sensors by designing functional groups, which has guiding significance for future work.

This work was supported by the National Natural Science Foundation of China (21975254, 91961115, 22171263), the National Natural Science Foundation from Fujian province (2021J02017, 2020J01109, 22175176), and Youth Innovation Promotion Association CAS (2018342).

Conflicts of interest

There are no conflicts to declare.

Notes and references

- 1 K. S. Novoselov, A. K. Geim, S. V. Morozov, D. Jiang, Y. Zhang, S. V. Dubonos, I. V. Grigorieva and A. A. Firsov, Science, 2004,
- 2 C. Tan, X. Cao, X. J. Wu, Q. He, J. Yang, X. Zhang, J. Chen, W. Zhao, S. Han, G. H. Nam, M. Sindoro and H. Zhang, Chem. Rev., 2017, 117, 6225.
- 3 Z. Wang, J. Qiu, X. Wang, Z. Zhang, Y. Chen, X. Huang and W. Huang, Chem. Soc. Rev., 2018, 47, 6128.
- 4 Q. Fu and X. Bao, Chem. Soc. Rev., 2017, 46, 1842.

- 5 W. Y. Chen, C. Yen, S. Xue, H. Wang and L. A. Stanciu, ACS Appl. Mater. Interfaces, 2019, 11, 34135.
- 6 P. M. Neema, A. M. Tomy and J. Cyriac, TrAC, Trends Anal. Chem., 2020, 124, 115797.
- 7 X. Sun, Y. Wang and Y. Lei, Chem. Soc. Rev., 2015, 22, 8019.
- 8 Y. Guo, X. Feng, T. Han, S. Wang, Z. Lin, Y. Dong and B. Wang, J. Am. Chem. Soc., 2016, 138, 10100.
- 9 Z. Zhai, S. Yang, M. Cao, L. Li, C. Du and S. Zang, Cryst. Growth Des., 2018, 18, 7173.
- 10 J. Qin, B. Ma, X. Liu, H. Lu, X. Dong, S. Zang and H. Hou, Dalton Trans., 2015, 44, 14594.
- 11 D. Voiry, A. Goswami, R. Kappera, C. Silva, D. Kaplan, T. Fujita, M. Chen, T. Asefa and M. Chhowalla., Nat. Chem., 2015, 7, 45.
- 12 F. Zhang, Y. Lu, D. Schulman, T. Zhang, K. Fujisawa, Z. Lin, Y. Lei, A. Elias, S. Das, S. Sinnott and M. Terrones, Sci. Adv., 2019, 5, eaav5003.
- 13 E. E. Benson, H. Zhang, S. A. Schuman, S. U. Nanayakkara, N. D. Bronstein, S. Ferrere, J. L. Blackburn and E. M. Miller., I. Am. Chem. Soc., 2018, 140, 441.
- 14 Y. Z. Li, J. Shu, Q. Q. Huang, K. Chiranjeevulu, P. N. Kumar, G. E. Wang, W. H. Deng, D. Tang and G. Xu, Chem. Commun., 2019, 55, 10444.
- 15 Y. Li, X. Jiang, Z. Fu, Q. Huang, G. Wang, W. Deng, C. Wang, Z. Li, W. Yin, B. Chen and G. Xu, Nat. Chem., 2020, 11, 261.
- 16 H. Jiang, L. Cao, Y. Li, L. We., X. Ye, W. Deng, X. Jiang, G. Wang and G. Xu, Chem. Commun., 2020, 56, 5366.
- 17 C. Lavenn, N. Guillou, M. Monge, D. Podbevsek, G. Ledoux, A. Fateeva and A. Demessence, Chem. Commun., 2016, 52, 9063.
- 18 O. Veselska, L. Okhrimenko, N. Guillou, D. Podbevsek, G. Ledoux, C. Dujardin, M. Monge, D. M. Chevrier, R. Yang, P. Zhang, A. Fateeva and A. Demessence, J. Mater. Chem. C, 2017, 5, 9843.
- 19 O. Veselska, D. Podbevsek, G. Ledoux, A. Fateeva and A. Demessence, Chem. Commun., 2017, 53, 12225.
- 20 O. Veselska, L. Cai, D. Podbevsek, G. Ledoux, N. Guillou, G. Pilet, A. Fateeva and A. Demessence, Inorg. Chem., 2018, 57, 2736.
- 21 C. Gong, X. Hu, Z. Han, X. Liu, M. Yang and S. Zang, Chem. Commun., 2022, 58, 1788.
- 22 J. Troyano, J. Perles, P. Amo-Ochoa, J. Ignacio Martínez, M. C. Gimeno, V. Fernández-Moreira, F. Zamora and S. Delgado, Chem. - Eur. J., 2016, 22.
- 23 J. Troyano, O. Castillo, J. I. Martínez, V. Fernández-Moreira, Y. Ballesteros, D. Maspoch, F. Zamora and S. Delgado., Adv. Funct. Mater., 2018, 28, 1704040.
- 24 D. Singha, S. Bhattacharya, P. Majee, S. Mondal, M. Kumar and P. Mahata, J. Mater. Chem. C, 2014, 2, 20908.
- 25 S. Liu, D. Luo, N. li, W. Zhang, J. Lei, N. Li and H. Luo, ACS Appl. Mater. Interfaces, 2016, 8, 21700.
- 26 W. Guan, W. Zhou, J. Lu and C. Lu, Chem. Soc. Rev., 2015, 44, 6981.
- 27 X. Jiang, Y. Liu, P. Wu, L. Wang, Q. Wang, G. Zhu, X. Lia and J. Wang, RSC Adv., 2014, 4, 47357.
- 28 D. Singha and P. Mahata, RSC Adv., 2015, 5, 28092.
- 29 Y. Wang, Y. Xua, Z. Yang, X. Zhang, Y. Hu and R. Yang, J. Colloid Interface Sci., 2021, 598, 474.
- 30 M. Faheem, S. Aziz, X. Jing, T. Ma, J. Du, F. Sun, Y. Tian and G. Zhua, J. Mater. Chem. A, 2019, 7, 27148.
- 31 Y. Wen, G. Wang, X. Jiang, X. Ye, W. Li and G. Xu, Angew. Chem., Int. Ed., 2021, 60, 1.
- 32 Y. Salinas, R. Martinez-Manez, M. D. Marcos, F. Sancenon, A. M. Castero, M. Parra and S. Gil, Chem. Soc. Rev., 2012, 41, 1261.
- 33 S. Pramanik, C. Zheng, X. Zhang, T. J. Emge and J. Li, J. Am. Chem. Soc., 2011, 133, 4153.
- 34 B. Wang, X. Lv, D. Feng, L. Xie, J. Zhang, M. Li, Y. Xie, J. Li and H. Zhou, J. Am. Chem. Soc., 2016, 138, 6204.
- 35 H. Sohn, M. J. Sailor, D. Magde and W. C. Trogler, J. Am. Chem. Soc., 2003, 125, 3821.
- 36 X. Jiang, Y. Liu, P. Wu, L. Wang, Q. Wang, G. Zhu, X. Li and J. Wang, RSC Adv., 2014, 4, 47357.
- 37 X. Sun, Y. Wang and Y. Lei, Chem. Soc. Rev., 2015, 44, 8019.
- 38 W. Wei, X. Huang, K. Chen, Y. Tao and X. Tang, RSC Adv., 2012, 2, 3765.
- 39 S. S. Nagarkar, B. Joarder, A. T. K. Chaudhari, S. Mukherjee and S. K. Ghosh, Angew. Chem., Int. Ed., 2013, 52, 2881.